Quantum Oscillations of the Positive Longitudinal Magnetoconductivity: A Fingerprint for Identifying Weyl Semimetals

Ming-Xun Deng, G. Y. Qi, R. Ma, R. Shen, Rui-Qiang Wang, L. Sheng, and D. Y. Xing

Phys. Rev. Lett. **122**, 036601 — Published 24 January 2019

DOI: 10.1103/PhysRevLett.122.036601

Quantum Oscillations of The Positive Longitudinal Magnetoconductivity: a Fingerprint for Identifying Weyl Semimetals

Ming-Xun Deng[1,2], G. Y. Qi [1], R. Ma [3], R. Shen[1,4], Rui-Qiang Wang[2], L. Sheng[1,4,*] and D. Y. Xing[1,4†]
[1] *National Laboratory of Solid State Microstructures and Department of Physics, Nanjing University, Nanjing 210093, China*
[2] *Laboratory of Quantum Engineering and Quantum Materials, ICMP and SPTE, South China Normal University, Guangzhou 510006, China*
[3] *Jiangsu Key Laboratory for Optoelectronic Detection of Atmosphere and Ocean, Nanjing University of Information Science and Technology, Nanjing 210044, China*
[4] *Collaborative Innovation Center of Advanced Microstructures, Nanjing University, Nanjing 210093, China*
(Dated: January 4, 2019)

Weyl semimetals (WSMs) host charged Weyl fermions as emergent quasiparticles. We develop a unified analytical theory for the anomalous positive longitudinal magnetoconductivity (LMC) in a WSM, which bridges the gap between the classical and ultra-quantum approaches. More interestingly, the LMC is found to exhibit periodic-in-$1/B$ quantum oscillations, originating from the oscillations of the nonequilibrium chiral chemical potential. The quantum oscillations, superposed on the positive LMC, are a remarkable fingerprint of a WSM phase with chiral anomaly, whose observation is a valid criteria for identifying a WSM material. In fact, such quantum oscillations were already observed by several experiments.

PACS numbers: 72.10.-d, 73.43.Qt, 75.45.+j

Weyl semimetals (WSMs), whose low-energy excitations are Weyl fermions [1] carrying charges, have recently spurred intensive and innovative research in the field of condensed matter physics [2–8]. The ultra-high mobility and spectacular transport properties of the charged Weyl fermions can find applications in high-speed electronic circuits and computors [9–11]. The low-energy spectrum of a WSM forms non-degenerate three-dimensional (3D) Dirac cones around isolated degenerate band touching points, referred to as Weyl points [2]. Weyl points with opposite chiralities, playing the parts of the source and sink of Berry curvature in momentum space, always come in pairs [12, 13]. The appearance of the Weyl points requires breaking either the spatial inversion or time-reversal symmetry. Weyl points with opposite chiralities in momentum space are connected by the nonclosed Fermi arc surface states. [2].

The WSM state was first realized experimentally in TaAs [14–16], following the theoretical predictions [17, 18], and later in several different compounds [10, 19–30]. WSMs display many anomalous transport properties, such as positive longitudinal magnetoconductivity (LMC), optical gyrotropy [31], planar Hall effect [32], all of which are induced by the chiral anomaly [13], and nonlocal quantum oscillations of the Fermi arc surface states [33]. The chiral anomaly, also termed as the Adler-Bell-Jackiw anomaly, means the violation of the separate number conservation laws of Weyl fermions of different chiralities. Parallel electric and magnetic fields can pump Weyl fermions between Weyl valleys of opposite chiralities, and create a population imbalance between them, therefore resulting in a positive LMC (or negative magnetoresistance). The anomalous LMC, as an exotic macroscopic quantum phenomenon, has been attracting intense experimental [10, 20–30] and theoretical [7, 34–37] interest.

In order to identify a WSM material, the ARPES experiments were used to directly observe the Weyl nodes and Fermi arcs [14–16, 19]. However, the ARPES identification is sometime limited by spectroscopic resolutions. Another widely-employed method is to measure the positive LMC induced by the chiral anomaly [10, 20–29]. The observation of the positive LMC is only a necessary condition for identifying the WSM phase, but not a sufficient condition. On the other hand, in the classical limit, $|E_F| \gg \hbar\omega_c$, an analytical formula for the anomalous LMC was derived in Refs. [35, 36], yielding $\Delta\sigma(B) \propto (B/E_F)^2$ with E_F the Fermi energy, ω_c the cyclotron frequency, and B the strength of magnetic field. In the opposite ultra-quantum limit, $|E_F| \ll \hbar\omega_c$, it was shown independently [35, 37] that $\Delta\sigma(B) \propto B$. While the above quadratic or linear field dependence of the positive LMC was suggested as an additional signature of a WSM, in experiments the simultaneous presence of negative field-dependent LMC due to destruction of weak anti-localization [10, 20–29] often makes comparison of experimental data with the theories equivocal. Besides, in the classical limit, Andreev and Spivak [38–40] recently claimed that positive LMC might also occur in some conventional conductors, by assuming that the disorder potential is smooth on the interatomic scale. Theoretical investigation of the anomalous LMC in the intermediate regime between the classical and ultra-quantum limits is still absent. It is urgent to develop a unified theory across the two limits by taking into account the interplay between the chiral anomaly and Landau quantization, and in particular to seek out a fingerprint identification of a WSM material based on transport measurements.

The main purpose of this Letter is twofold. First, integrating the Landau quantization with Boltzmann

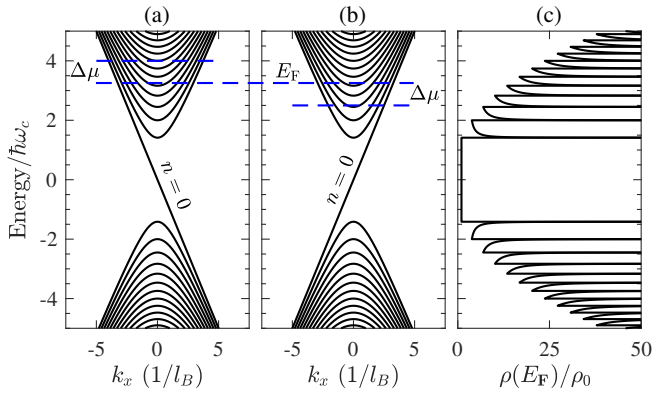

FIG. 1: The LLs in (a) $\chi = +$, and (b) $\chi = -$ Weyl valleys. (c) The DOS of the Weyl fermions (horizontal axis) as a function of normalized Fermi energy $E_F/\hbar\omega_c$ (vertical axis). Blue dashed lines in (a,b) are an enlarged illustration of the effect of chiral anomaly. In the steady state, the local chemical potentials in the two valleys shift upward and downward relative to E_F, respectively, by an equal amount $\Delta\mu$, indicating a transfer of charged fermions between the two valleys.

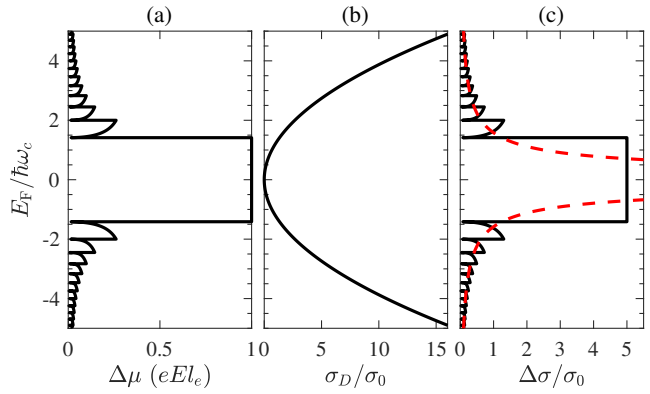

FIG. 2: (a) $\Delta\mu$, (b) σ_D, and (c) $\Delta\sigma(B)$ as functions of $E_F/\hbar\omega_c$ for $\tau_{inter} = 5\tau_{intra}$. The red dashed curve plotted in (c) is calculated from the classical formula (14). We set the magnetic field to be $B = 1T$, and define $\sigma_0 = \frac{2e^2}{h}\frac{e[B=1T]v_F\tau_{intra}}{h}$ as the unit of conductivity, for convenience.

equation, we derive a unified analytical formula for the anomalous LMC in a WSM, which is applicable to a broad range from the classical to ultra-quantum limit. It recovers the known results in the two opposite limits. More interestingly, we find that the anomalous positive LMC displays periodic-in-1/B quantum oscillations, originating from the oscillations of the nonequilibrium chiral chemical potential. Second, we propose that the quantum oscillations superposed on the positive LMC are an important fingerprint for identifying a WSM material with chiral anomaly, which was not disclosed in previous theories. Unlike the quadratic or linear field dependence, the quantum oscillations of the anomalous LMC will not be concealed by the presence of negative LMC related to weak anti-localization. In fact, such quantum oscillations were already observed by several experimental works, e.g., see Figs. 3(a,b) in Ref. [21], Fig. 2(d) in Ref. [26], Fig. 3(d) in Ref. [29], and Fig. 3 in Ref. [30].

Let us start by considering a 3D WSM, which has two Weyl points with opposite chiralities, labelled by $\chi = \pm$. When a magnetic field $\mathbf{B} = (B, 0, 0)$ is applied along the x direction, the continuum Hamiltonian for the low-energy electrons in a Weyl valley reads

$$H_\chi(\mathbf{k}) = \chi v_{\rm F}\left(\hbar\mathbf{k} + e\mathbf{A}\right)\cdot\boldsymbol{\sigma}\ , \tag{1}$$

where the electron charge is taken to be $-e$, $v_{\rm F}$ is the Fermi velocity, $\boldsymbol{\sigma} = (\sigma_x, \sigma_y, \sigma_z)$ are the Pauli matrices, $\mathbf{k}$ is the wave vector, and $\mathbf{A}$ is the vector potential defined by $\mathbf{B} = \nabla\times\mathbf{A}$. The Zeeman field is omitted, as it just causes a translation of k_x for this linearized Hamiltonian, and will not lead to observable effect. The energy spectrum can be solved exactly, yielding

$$\varepsilon_n^\chi(k_x) = \begin{cases} -\chi\hbar v_{\rm F}k_x & n = 0 \\ {\rm sgn}(n)\sqrt{2|n|(\hbar\omega_c)^2 + (\hbar v_{\rm F}k_x)^2} & n \neq 0 \end{cases} \tag{2}$$

with $\ell_B = \sqrt{\hbar/eB}$ as the magnetic length and $\omega_c = v_{\rm F}/\ell_B$. The degeneracy of each Landau level (LL) is equal to $\Omega_n^\chi = 1/2\pi\ell_B^2$ per unit cross-section. The longitudinal group velocity for the n-th LL is given by

$$v_{x,n}^\chi(k_x) = \frac{\partial\varepsilon_n^\chi(k_x)}{\hbar\partial k_x} = \begin{cases} -\chi v_{\rm F} & n = 0 \\ \hbar v_{\rm F}^2 k_x/\varepsilon_n^\chi(k_x) & n \neq 0 \end{cases}\ . \tag{3}$$

The LLs are plotted in Figs. 1(a) and 1(b), whose slopes correspond to group velocities $v_{x,n}^\chi(k_x)$. In each Weyl valley, the $n = 0$ LL is chiral, manifesting the chirality of the Weyl point, and all $n \neq 0$ LLs are achiral.

The two valleys have the identical density of states (DOS). The DOS at E_F of a single valley is given by $\rho(E_F) = \rho_0\Theta$, where $\rho_0 = 1/2\pi\ell_B^2 h v_F$, and

$$\Theta = 2\sum_{n=0}^{n_c}\frac{1}{\lambda_n} - 1\ , \tag{4}$$

with $\lambda_n = \sqrt{1 - 2|n|(\hbar\omega_c/E_{\rm F})^2}$. Here, $n_c = {\rm sgn}(E_F){\rm int}\left[E_F^2/2(\hbar\omega_c)^2\right]$ is the index of the highest (lowest) LL crossed by the Fermi level for $E_F > 0$ ($E_F < 0$). The DOS $\rho(E_F)$ is plotted in Fig. 1(c). It oscillates strongly with changing E_F due to the oscillating factor Θ. Whenever the top or bottom of a LL passes through E_F, i.e., at $E_F = {\rm sgn}(n)\sqrt{2|n|}\hbar\omega_c$ with $n \neq 0$, $\rho(E_F)$ diverges periodically, exhibiting van Hove singularities.

Upon application of an electric field $\mathbf{E} = (E, 0, 0)$ along the x direction, namely, $\mathbf{E} \parallel \mathbf{B}$, the linear-response steady-state electron distribution function for the n-th

LL in the χ valley in general takes the form

$$f_n^\chi(k_x) = f_0(\varepsilon_n^\chi) - f_0'(\varepsilon_n^\chi) g_n^\chi(k_x) \ , \tag{5}$$

where $f_0(\varepsilon_n^\chi) = 1/[e^{(\varepsilon_n^\chi - E_F)/k_BT} + 1]$ is the equilibrium distribution function, $f_0'(\varepsilon_n^\chi) = \partial f_0(\varepsilon_n^\chi)/\partial \varepsilon_n^\chi$, and $g_n^\chi(k_x)$ describes the deviation of the electron distribution function from $f_0(\varepsilon_n^\chi)$. The linearized Boltzmann equation reads

$$e v_{x,n}^\chi E = -\frac{g_n^\chi(k_x) - \overline{g}_\chi}{\tau_{intra}} - \frac{\overline{g}_\chi}{\tau_{inter}} \ , \tag{6}$$

with $\overline{g}_\chi = \langle g_n^\chi(k_x)\rangle_\chi$, where τ_{intra} and τ_{inter} stand for the transport relaxation times due to the electron intravalley and intervalley scattering by impurities. The scattering terms on the right-hand side of Eq. (6) account for the fact that the intravalley scattering can only relax the system toward local equilibrium within each valley, and the intervalley scattering is responsible for relaxation of the system toward the global equilibrium between the valleys. It is assumed that $\tau_{inter} \gg \tau_{intra}$, as the separation of the Weyl points in the Brillouin zone usually makes the intervalley scattering much weaker than intravalley scattering. Here, the average $\langle\cdots\rangle_\chi$ runs over all electron states at the Fermi level in the χ valley, defined as

$$\langle\cdots\rangle_\chi = \frac{\sum_n \frac{1}{2\pi\ell_B^2}\int \frac{dk_x}{2\pi}[-f_0'(\varepsilon_n^\chi)](\cdots)}{\sum_n \frac{1}{2\pi\ell_B^2}\int \frac{dk_x}{2\pi}[-f_0'(\varepsilon_n^\chi)]} \ . \tag{7}$$

From Eq. (6), it is easy to obtain a formal solution for $g_n^\chi(k_x)$,

$$g_n^\chi(k_x) = -e v_{x,n}^\chi E \tau_{intra} + \left(1 - \frac{\tau_{intra}}{\tau_{inter}}\right)\overline{g}_\chi \ . \tag{8}$$

The unknown $\overline{g}_\chi$ on the right hand side of Eq. (8) can be solved self-consistently by averaging the both sides of Eq. (8) at the Fermi level, yielding

$$\overline{g}_\chi = -\langle v_{x,n}^\chi\rangle_\chi e E \tau_{inter} \ . \tag{9}$$

We notice that only the chiral $n = 0$ LL in the χ valley makes nonzero contribution to $\langle v_{x,n}^\chi\rangle_\chi$ and in turn to $\overline{g}_\chi$. $\overline{g}_+$ and $\overline{g}_-$ are equal in magnitude and opposite in sign, and so we denote $\overline{g}_+ \equiv -\overline{g}_- = \Delta\mu$.

By substitution of Eq. (9) into Eq. (8), we obtain

$$g_n^\chi(k_x) = -e v_{x,n}^\chi E \tau_{intra} + \chi\Delta\mu \ . \tag{10}$$

The term linear in $\tau_{intra}/\tau_{inter} \ll 1$ in Eq. (8) can now be omitted. According to Eq. (5), the second term in Eq. (10) corresponds to the nonequilibrium local chemical potentials in the $\chi = \pm$ valleys relative to E_F. Therefore, $\Delta\mu$ is called the chiral chemical potential [41]. A nonzero $\Delta\mu$, as illustrated by the blue lines in Fig. 1(a,b), indicates that an imbalance of carrier density is established between the two Weyl valleys.

The electrical current density is given by

$$j_x = \frac{-e}{2\pi\ell_B^2}\sum_{\chi,n}\int v_{x,n}^\chi(k_x) g_n^\chi(k_x)\,[-f_0'(\varepsilon_n^\chi)]\,\frac{dk_x}{2\pi} \ . \tag{11}$$

Substituting Eq. (10) into Eq. (11), we divide the conductivity into two parts $\sigma(B) \equiv j_x/E = \sigma_D + \Delta\sigma(B)$. The zero-field Drude conductivity is given by

$$\sigma_D = \frac{n_e e^2}{\hbar k_F} v_F \tau_{intra} \ , \tag{12}$$

with $k_F = |E_F|/\hbar v_F$ and $n_e = \frac{1}{3\pi^2}k_F^3$ as the carrier density.

At zero temperature, we can obtain $\Delta\mu = eEl_e/\Theta$ with $l_e = v_F\tau_{inter}$. To the leading order in $\tau_{intra}/\tau_{inter} \ll 1$, the LMC $\Delta\sigma(B) \equiv [\sigma(B) - \sigma_D]$ is derived to be

$$\Delta\sigma(B) = \frac{2e^2}{h}\frac{eBv_F\tau_{inter}}{h}\frac{1}{\Theta} \ . \tag{13}$$

This quantum formula is the central result of our work. $\Delta\sigma(B)$ contains an oscillating factor $1/\Theta$, which is introduced in Eq. (4). Another feature of $\Delta\sigma(B)$ is that it is proportional to the intervalley relaxation time τ_{inter}, because the nonequilibrium chiral chemical potential can only relax via intervalley scattering [35, 36].

In Figs. 2(a-c), we plot the calculated $\Delta\mu$, σ_D and $\Delta\sigma(B)$ as functions of the normalized Fermi energy $E_F/\hbar\omega_c$. As mentioned above, $\Delta\mu$ is inversely proportional to the electron DOS. At $E_F = \mathrm{sgn}(n)\sqrt{2|n|}\hbar\omega_c$ with $n \neq 0$, where the DOS diverges, $\Delta\mu$ vanishes periodically. $\Delta\sigma(B)$ actually originates from $\Delta\mu$, so that they exhibit synchronous oscillations. For $|E_F| \gg \hbar\omega_c$, if we neglect the oscillations in $\Delta\sigma(B)$, by assuming E_F not very close to $\mathrm{sgn}(n)\sqrt{2|n|}\hbar\omega_c$ with $n \neq 0$, we can replace the summation over n in Θ by an integral $\sum_{n=1}^{n_c} \to \int_0^{n_c} dn$, and then obtain $\Theta \simeq 2(E_F/\hbar\omega_c)^2$. In this case, Eq. (13) reduces to

$$\Delta\sigma(B) = \frac{e^2}{4\pi^2\hbar}\frac{(eB)^2 v_F^2}{E_F^2} v_F\tau_{inter} \ , \tag{14}$$

which recovers the classical formula obtained in Refs. [35, 36], and its result is also plotted in Fig. 2(c) as a red dashed line. The classical formula does not show any oscillations, and is approximately consistent with the envelope of the quantum formula for $|E_F| \gg \hbar\omega_c$. For relatively strong magnetic field, $|E_F| \lesssim \hbar\omega_c$, however, the two formulas deviate from each other substantially. In the strong-field regime, for $|E_F| < \sqrt{2}\hbar\omega_c$, where the Fermi level crosses only the $n = 0$ LLs, we have $n_c = 0$ and $\Theta = 1$. In this limiting case, the quantum formula (13) can be simplified to

$$\Delta\sigma(B) = \frac{e^2}{2\pi^2\hbar}\frac{eBv_F\tau_{inter}}{\hbar} \ . \tag{15}$$

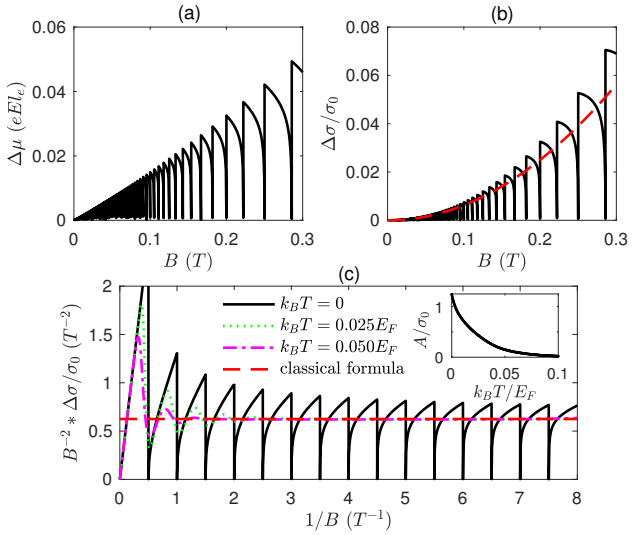

FIG. 3: (a) $\Delta\mu$, and (b) $\Delta\sigma(B)$ versus the magnetic field B at zero temperature. (c) The data of (b) are replotted to show the periodic-in-$1/B$ dependence of $\Delta\sigma(B)$ (black line), and the results at two finite temperatures are also shown. The red dashed lines in (b) and (c) are obtained from classical formula (14). Here, σ_0 is defined in Fig. 2, and the Fermi energy is set to $E_F = 2\hbar\omega_c|_{B=1T} = 2v_F\sqrt{e\hbar[B=1T]}$. Inset: the oscillation amplitude A of the LMC as a function of temperature.

This formula is in agreement with that derived in Ref. [35] in the ultra-quantum limit (except for an extra prefactor $1/2$ in the latter). The unsaturated LMC becomes linearly scaled with B, being independent of E_F.

Apart from varying electron Fermi energy E_F, the quantum oscillations in the LMC predicted by Eq. (13) can also be observed in experiments conveniently by varying the magnetic field B. In Figs. 3(a) and (b), we plot $\Delta\mu$ and $\Delta\sigma(B)$ as functions of B. We see that both of them oscillate with B. As has been discussed, both $\Delta\mu$ and $\Delta\sigma(B)$ drop to zero at $E_{\rm F} = {\rm sgn}(n)\sqrt{2|n|(\hbar\omega_c)^2}$ with $|n| \neq 0$, or say, at $1/B = 2|n|e\hbar\,(v_F/E_F)^2$. Therefore, $\Delta\sigma(B)$ is periodic-in-$1/B$ with the period

$$\Delta\left(\frac{1}{B}\right) = 2e\hbar\left(\frac{v_{\rm F}}{E_{\rm F}}\right)^2 . \qquad (16)$$

For the parameters chosen in Fig. 3, $\Delta\,(1/B) = 0.5/T$. In Fig. 3(c), we replot the LMC as $B^{-2}\Delta\sigma(B)/\sigma_0$ versus $1/B$. We see that the constant oscillation period is indeed $0.5/T$. Moreover, the envelope of $\Delta\sigma(B)$ deviates appreciably from the B^2 dependence predicted by the classical formula for relatively small $1/B$ (large B).

For finite temperatures, we perform numerical calculations. We focus on the parameter regime, $k_BT \ll \sqrt{2}\hbar\omega_c \leq |E_F|$, which is essentially the necessary condition for observing apparent quantum oscillations of the LMC. In this regime, because $k_BT \ll |E_F|$, we can neglect the temperature dependence in the equilibrium chemical potential for simplicity. The nonequilibrium chiral chemical potential $\Delta\mu$ and the LMC are calculated by using Eqs. (9)-(11). The calculated results for two finite temperatures are also shown in Fig. 3(c). We see that the quantum oscillations become weaker gradually and finally fade out with increasing temperature, in agreement with experimental observations [21, 26, 29, 30]. Furthermore, from Fig. 3(c), it is found that for a fixed magnetic field strength, the LMC can increase or decrease with increasing temperature, depending on whether the field strength is near a valley or near a peak. This could explain the non-unified temperature dependencies of the LMC observed in Ref. [30]. In the inset of Fig. 3, the oscillation amplitude A of the LMC, namely, the difference between the highest peak and the nearest valley of $\Delta\sigma(B)$, is plotted as a function of temperature. The amplitude decreases monotonically with temperature, exhibiting Lifshitz-Kosevich type behavior.

Finally, we also suggest to study the optical conductivity of a WSM in an *ac* driving electric field with frequency ω. In the low-frequency regime, i.e., $\omega\tau_{inter} \ll 1$, the chiral chemical potential $\Delta\mu$ can keep up with the oscillation of the *ac* field, and oscillates synchronically, so that the LMC induced by the chiral anomaly still happens, similarly to the *dc* case. However, in the high-frequency regime, $\omega\tau_{inter} \gg 1$, there is no enough time for $\Delta\mu$ to build up and relax each cycle, and so the LMC is expected to vanish. Therefore, with increasing ω, it will be interesting to observe the transitional change of the LMC from a finite value to vanishing around $\omega \sim 1/\tau_{inter}$, which provides a possible way to measure the key parameter τ_{inter} directly. For typical values of the transport relaxation time, such a change is estimated to occur in the microwave or infrared frequency range.

In summary, we have derived a unified quantum formula, Eq. (13), for the chiral-anomaly-induced positive LMC in WSMs. It predicts periodic-in-$1/B$ quantum oscillations of the positive LMC, as a remarkable fingerprint for identifying a WSM material. The quantum oscillations of the anomalous LMC are quite different from the usual SdH oscillations, the latter appearing in the transverse conductivity with $\mathbf{E} \perp \mathbf{B}$. The quantum oscillations superposed on the positive LMC are a valuable criterion for identifying a WSM material. We have confined ourselves to the limit of weak impurity scattering, where the leading-order effect of the impurity potential can generally be included by the scattering terms of the Boltzmann equation. The effect of relatively strong impurity potential will be similar to that of finite temperatures, as shown in Fig. 3(c). Increasing the strength of impurity potential will gradually decrease and eventually destroy the quantum oscillations. However, we expect that the quantum oscillations, as an intrinsic property of the anomalous LMC, will emerge in high-quality WSMs at sufficiently strong magnetic fields and low tempera-

tures.

ACKNOWLEDGMENTS

This work was supported by the State Key Program for Basic Researches of China under Grants No. 2015CB921202 (L.S.), and No. 2017YFA0303203 (D.Y.X.), the National Natural Science Foundation of China under Grants No. 11674160 (L.S.), No. 11574155 (R.M.), and the Key Program for Guangdong NSF of China under Grant No. 2017B030311003 (R.-Q.W.).

* Electronic address: shengli@nju.edu.cn
† Electronic address: dyx@nju.edu.cn

[1] H. Weyl, I. Zeitschr. Phys. **56**, 330 (1929).
[2] X. Wan, A. M. Turner, A. Vishwanath, and S. Y. Savrasov, Phys. Rev. B **83**, 205101 (2011).
[3] G. Xu, H. Weng, Z. Wang, X. Dai, and Z. Fang, Phys. Rev. Lett. **107**, 186806 (2011).
[4] A. A. Burkov and L. Balents, Phys. Rev. Lett. **107**, 127205 (2011).
[5] K.-Y. Yang, Y.-M. Lu, and Y. Ran, Phys. Rev. B **84**, 075129 (2011).
[6] G. B. Halász and L. Balents, Phys. Rev. B **85**, 035103 (2012).
[7] H.-J. Kim, K.-S. Kim, J.-F. Wang, M. Sasaki, N. Satoh, A. Ohnishi, M. Kitaura, M. Yang, and L. Li, Phys. Rev. Lett. **111**, 246603 (2013).
[8] P. Hosur and X. Qi, Comptes Rendus Physique **14**, 857 (2013).
[9] M. N. Ali, J. Xiong, S. Flynn, J. Tao, Q. D. Gibson, L. M. Schoop, T. Liang, N. Haldolaarachchige, M. Hirschberger, N. Ong, et al., Nature **514**, 205 (2014).
[10] C. Shekhar, A. K. Nayak, Y. Sun, M. Schmidt, M. Nicklas, I. Leermakers, U. Zeitler, Y. Skourski, J. Wosnitza, Z. Liu, et al., Nat. Phys. **11**, 645 (2015).
[11] S. A. Parameswaran, T. Grover, D. A. Abanin, D. A. Pesin, and A. Vishwanath, Phys. Rev. X **4**, 031035 (2014).
[12] G. E. Volovik, *The universe in a helium droplet*, vol. 117 (Oxford University Press on Demand, 2003).
[13] H. Nielsen and M. Ninomiya, Phys. Lett. B **130**, 389 (1983).
[14] S.-Y. Xu, I. Belopolski, N. Alidoust, M. Neupane, G. Bian, C. Zhang, R. Sankar, G. Chang, Z. Yuan, C.-C. Lee, et al., Science **349**, 613 (2015).
[15] B. Q. Lv, H. M. Weng, B. B. Fu, X. P. Wang, H. Miao, J. Ma, P. Richard, X. C. Huang, L. X. Zhao, G. F. Chen, et al., Phys. Rev. X **5**, 031013 (2015).
[16] B. Q. Lv, N. Xu, H. M. Weng, J. Z. Ma, P. Richard, X. C. Huang, L. X. Zhao, G. F. Chen, C. E. Matt, F. Bisti, et al., Nat. Phys. **11**, 724 (2015).
[17] S.-M. Huang, S.-Y. Xu, I. Belopolski, C.-C. Lee, G. Chang, B. Wang, N. Alidoust, G. Bian, M. Neupane, C. Zhang, et al., Nature Communications **6**, 7373 (2015).
[18] H. Weng, C. Fang, Z. Fang, B. A. Bernevig, and X. Dai, Phys. Rev. X **5**, 011029 (2015).
[19] L. X. Yang, Z. K. Liu, Y. Sun, H. Peng, H. F. Yang, T. Zhang, B. Zhou, Y. Zhang, Y. F. Guo, M. Rahn, et al., Nat. Phys. **11**, 728 (2015).
[20] J. Xiong, S. K. Kushwaha, T. Liang, J. W. Krizan, M. Hirschberger, W. Wang, R. J. Cava, and N. P. Ong, Science **350**, 413 (2015).
[21] C.-Z. Li, L.-X. Wang, H. Liu, J. Wang, Z.-M. Liao, and D.-P. Yu, Nat. Commun. **6**, 10137 (2015).
[22] Y. Wang, E. Liu, H. Liu, Y. Pan, L. Zhang, J. Zeng, Y. Fu, M. Wang, K. Xu, Z. Huang, et al., Nat. Commun. **7**, 13142 (2016).
[23] Y.-Y. Lv, X. Li, B.-B. Zhang, W. Y. Deng, S.-H. Yao, Y. B. Chen, J. Zhou, S.-T. Zhang, M.-H. Lu, L. Zhang, et al., Phys. Rev. Lett. **118**, 096603 (2017).
[24] X. Huang, L. Zhao, Y. Long, P. Wang, D. Chen, Z. Yang, H. Liang, M. Xue, H. Weng, Z. Fang, et al., Phys. Rev. X **5**, 031023 (2015).
[25] H. Li, H. He, H.-Z. Lu, H. Zhang, H. Liu, R. Ma, Z. Fan, S.-Q. Shen, and J. Wang, Nat. Commun. **7**, 10301 (2016).
[26] C.-L. Zhang, S.-Y. Xu, I. Belopolski, Z. Yuan, Z. Lin, B. Tong, G. Bian, N. Alidoust, C.-C. Lee, S.-M. Huang, et al., Nat. Commun. **7**, 10735 (2016).
[27] Y. Zhao, H. Liu, J. Yan, W. An, J. Liu, X. Zhang, H. Wang, Y. Liu, H. Jiang, Q. Li, et al., Phys. Rev. B **92**, 041104(R) (2015).
[28] X.-C. Pan, Y. Pan, J. Jiang, H. Zuo, H. Liu, X. Chen, Z. Wei, S. Zhang, Z. Wang, X. Wan, et al., Frontiers of Physics **12**, 127203 (2017).
[29] J. Du, H. Wang, Q. Mao, R. Khan, B. Xu, Y. Zhou, Y. Zhang, J. Yang, B. Chen, C. Feng, et al., Sci. China-Phys. Mech. Astron. **59**, 657406 (2016).
[30] C.-L. Zhang, B. Tong, Z. Yuan, Z. Lin, J. Wang, J. Zhang, C.-Y. Xi, Z. Wang, S. Jia, and C. Zhang, Phys. Rev. B **94**, 205120 (2016).
[31] P. Goswami, G. Sharma, and S. Tewari, Phys. Rev. B **92**, 161110 (2015).
[32] S. Nandy, G. Sharma, A. Taraphder, and S. Tewari, Phys. Rev. Lett. **119**, 176804 (2017).
[33] A. C. Potter, I. Kimchi, and A. Vishwanath, Nat. Commun. **5**, 5161 (2014).
[34] V. Aji, Phys. Rev. B **85**, 241101 (2012).
[35] D. T. Son and B. Z. Spivak, Phys. Rev. B **88**, 104412 (2013).
[36] A. A. Burkov, Phys. Rev. B **91**, 245157 (2015).
[37] X. Xiao, K. T. Law, and P. A. Lee, Phys. Rev. B **96**, 165101 (2017).
[38] A. V. Andreev and B. Z. Spivak, Phys. Rev. Lett. **120**, 026601 (2018).
[39] See the Supplemental Material [url] for a discussion about the theory of Andreev and Spivak, which includes Ref. [40].
[40] T. Liang, Q. Gibson, M. N. Ali, M. Liu, R. J. Cava, and N. P. Ong, Nature Materials **14**, 280 (2014).
[41] A. Yamamoto, Phys. Rev. Lett. **107**, 031601 (2011).